Peer-reviewed version available at *Metals* **2019**, *9*, 1074; doi:10.3390/met9101074

Effects of Al_2O_3 Addition on the Microstructure and Properties of CoCr Alloys

Qin Hong, Peikang Bai *, Jianhong Wang

College of Materials Science and Engineering
North University of China
Taiyuan, Shanxi, 030051, China

Abstract

In typical Cobalt-chromium (CoCr) alloys powders, aluminum oxide (Al_2O_3) powder can be added. In the present study, we successfully prepared alloyed samples of various powder ratios by laser cladding, and analyzed their microstructure and carbide structural characteristics, including microhardness, biological properties, morphology (using scanning electron microscopy), and crystal structure (using X-ray powder diffraction). Elemental distribution was also determined by energy-dispersive X-ray spectral analysis. The results showed that Al_2O_3 addition caused the alloy to change from slender columnar crystals to columnar grains similar, to equiaxed grains. In addition, Al_2O_3 agglomeration zones appeared, and carbide structures were altered. The mechanism of the observed performance changes was also analyzed.

Keywords: CoCr alloy; Microstructure; Powder modified; Al_2O_3

*Correspondingauthor：baipeikang@nuc.edu.cn

Peer-reviewed version available at Metals 2019, 9, 1074; doi:10.3390/met9101074

1. Introduction

The development of dental restoration has always been closely related to the progress of oral materials. Finding the most suitable materials and manufacturing techniques has always been the interest of dentists. In recent years, the use of all-ceramic restorations has been increasing in terms of oral repair materials, but their application has been impaired due to their high melting point and hardness, which impedes machining in terms of cutting and plasticity[1]. Therefore, metal-based medical materials are currently the first choice of dental prosthetic materials[2]. Cobalt-chromium (CoCr) alloys are cost-effective, and enjoy good physical and mechanical properties and good biocompatibility[3-5]. They are therefore used in a wide range of applications in the oral repair field, and remain one of the most commonly used materials in clinical practice.

CoCr alloys have been the focus of many studies. For example, Wiper *et al*. have and studied the effects of metal-porcelain bonding properties in porcelain teeth, including the metal-porcelain bonding strength that was tested using the international standard IS09693:1999. They found that the metal-ceramic bond strength of metal liners produced by 3D printing were effectively improved, and that the alloy properties were better than those of alloys produced by casting [6-8]. Hedberg *et al*. found that the rapid cooling in the selective laser melting (SLM) technique, led to the formation of a molybdenum (Mo)-rich phase in medical cobalt-chromium (CoCr)Mo alloys. A large proportion of hexagonal close-packed-type $Cr_{23}C_6$ particle phases were formed on the surface, effectively reducing the alloy's ion release, with the special

Peer-reviewed version available at Metals 2019, 9, 1074; doi:10.3390/met9101074

texture of the molten pool changing the corrosion resistance of these materials[9]. Second-phase particles with a size of <10 μm were found to effectively improve CoCrMo alloy mechanical properties[10].

In addition, the processing technology of CoCr alloys, their microstructure, and properties under different processes have extensively been studied[2,11-14], including a large number of studies on heat treatment processes and surface modification of CoCr alloys[15-18]. Cast CoCr alloys with coarse microstructure and solidification defects have been reported[19]. One of the major advantages of SLM technology, compared to foundry technology, is that the microstructures of CoCr alloys prepared under this technique are small. To date, there have been few studies on the preparation of CoCr alloys by laser cladding technology.

In recent years, increasing research has been performed on the preparation of metallic materials by laser cladding technology, and it has been found that the manufacturing accuracy is basically the same as SLM technology[20]. Because of the smaller dentures that laser cladding technology affords. Our present study uses laser cladding technology to make alloy materials and provide more methods for denture production.

Microalloying has always been a hot topic in material research. Making microalloyed elements fully exert their strengthening effects has a direct relationship to the alloy itself and elemental additions. Few studies have focused on the use of carbides for the modification of CoCr alloy powders. Al_2O_3 is the main material commonly used for blasting CoCr alloys[21,22]. Hagihara *et al*. found that Al_2O_3

Peer-reviewed version available at Metals 2019, 9, 1074; doi:10.3390/met9101074

addition results in a significant change in the structure of single crystals during directional solidification of CoCr alloy, ultimately increasing alloy strength[23]. The main goal of the present study is to further examine the modification of CoCr powder by Al_2O_3 powder addition. Original and modified powders were processed by single laser cladding forming, and their phases and microstructures were characterized by scanning electron microscopy (SEM) and X-ray powder diffraction (XRD). The mechanical properties of the two samples were also tested and compared to those of traditional CoCr alloy carbide in terms of the alloy morphology and the improvement in mechanical properties. This study provides a theoretical and technical reference for modification of existing CoCr powder applications.

2. Materials and method

The CoCr alloy used in this experiment was a CoCr-0404 alloy powder, produced by Renishaw Co,Inc. (Gloucestershire, UK). The mass fraction of Cr, Mo, Si, Mn, Fe and C are 29.5%, 5.3%, 0.7%, 0.5%, 0.4% and 1.2%, respectively. The powder had particle size that ranged from 10.3 to 31.2 μm, a density of 8.3 g/cm^3, and a melting point of 1380°C.

2.1 Preparation of sintered powder

Six groups of mixed powder were prepared by adding 2.5%, 5%, 7.5% and 10% Al_2O_3 to CoCr alloy, respectively. Each group of powder is placed in an Al_2O_3 crucible with a depth of 10 mm. Then, the crucible was baked in an oven at 90°C for 3 h. The powder particle size was measured using a Mastersizers 2000 laser particle size analyzer (Malvern Instruments Ltd., Worcestershire, UK). The surface morphology of the powder particles was observed under a KYKY-EM6200 tungsten

filament-quipped scanning electron microscope (SEM; KYKY Technology Co., Ltd., Beijing, China). The powder was measured for powder liquidity (time) and bulk density, in accordance with the standard methodology GB/T 1482-2010 "Determination of metal powder fluidity of the funnel method (Hall flowmeter)", and GB/T 1479.1-2011 "Determination of bulk metal powder density Part 1: funnel method".

2.2 Sample preparation

The experiment was carried out on a 4.0 KW LDF4000-100 fiber semiconductor laser (Laserline GmbH, Mülheim-Kärlich, Germany). A previous series of experiments determined the best process parameters : Laser output power $P \leq 1000$ W, scanning speed $V \leq 4$ mm/s, spot diameter $R \leq 2$ mm, laser scanning time 3 s. CoCr alloy test parts were obtained after scanning the horizontal cross-section parallel to the scanning direction of the line cutting and mosaic.

2.3 Microstructural analysis

For metallographic etching, samples were ground and polished with Murakami's reagent (potassium ferricyanide 10 g, sodium hydroxide 10 g, and deionized water 100 ml) heated to corrosion. The specific method involved soaking a sample in 20 ml of nitric acid + 3 drops of hydrofluoric acid solution for 10 to 80 h, then placing it for corrosion in Murakami's reagent at 90° C for 20 min. The samples were observed microscopically, using an AXIO ScopeA1 optical microscope (Carl Zeiss Microscopy GmbH, Göttingen, Germany). The microstructure of the specimen was observed using a HitachiSU5000 thermal field emission scanning electron microscope. The sample

phase composition was analyzed using a D/max-Rb XRD apparatus (Rigaku Corp., Tokyo, Japan).

2.4 Mechanical properties

In this experiment, the microhardness of several samples was tested on a Vickers hardness tester (DHV-1000, Shanghai Shangcai Testing Machine Co., Ltd., Shanghai, China) with a load of 0.98 N, and dwell time of 15 s. The measurement was done every 1 mm in the vertical direction of the cross-section.

According to the GB/T228.1-2010 standard methodology, the tensile properties of the specimens were tested on an electronic universal testing machine E43.504 (MTS Systems Corp., Eden Prairie, MN, USA). The tensile strength test was carried out at room temperature at a rate of 0.5 mm/min.

3. Results and discussion

3.1 Alloy powder microstructure and phase analysis

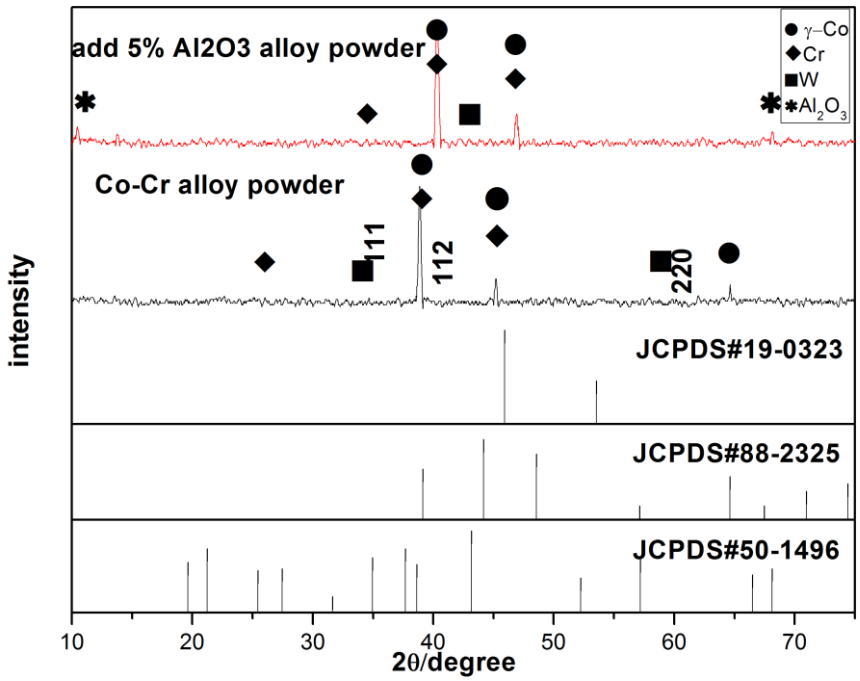

Fig. 1. XRD patterns of original and modified powders.

The analysis of XRD diffraction peaks of the CoCr alloy powder, showed that the main peak of the powder appears at 38–39°, and that the main phase was face-centered cubic (fcc)- γ-Co phase (Fig. 1). The standard cell parameters a and fcc-γ phase were a = 0.35447 ±0.0002 (ICDD card number 15-806) and the surface indices at γ (111), γ (112), and γ (220) matched. After adding Al_2O_3, the main peak of the composite powder appeared at 40–42°.

XRD data was further analyzed and it was observed that the main phase did not change substantially after Al_2O_3 addition, but the Al_2O_3 phase was identified. The main peak of the diffraction spectrum shifted upon the addition, which according to Bragg's Law, is attributed to structural changes in the unit cell, which cause the change in the diffraction peak positions. This shows that the interplanar spacing and lattice constant have become smaller, which would affect the power's deformation performance.

The powder's particle morphology remained almost spherical without Al_2O_3 addition, while smaller particles appeared with Al_2O_3 addition, compared to samples to which Al_2O_3 was not added (Fig. 2). The smaller sized particles had higher specific surface energy and melting enthalpy, and they melted rapidly under laser action. They also had good filling effects in gaps between large particles, such that the bulk density of the powder increased. This reduced the void defects inside the formed parts and improved their mechanical properties and surface quality.

Further analysis of the powder properties showed that the Al_2O_3 powder had a particle size distribution between 9.2 and 33.5 μm, a flowability of 22.10 s/50 g, and a

Preprints (www.preprints.org) | NOT PEER-REVIEWED | Posted: 2 September 2019 doi:10.20944/preprints201909.0025.v1

Peer-reviewed version available at Metals 2019, 9, 1074; doi:10.3390/met9101074

bulk density > 4.2 g/cm^3, which satisfies the general requirements of the process of laser cladding forming.

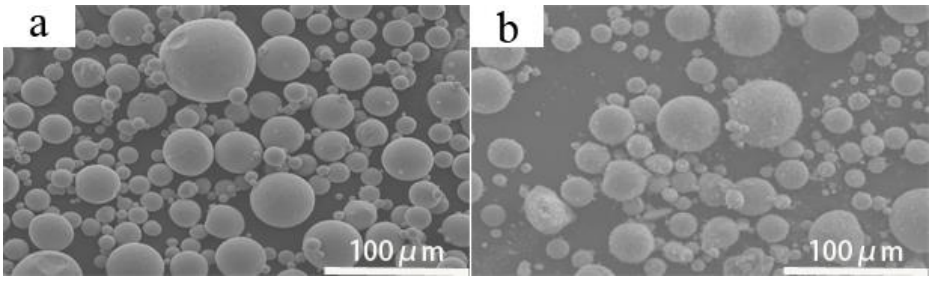

Fig. 2. Powder particle morphology: cobalt chromium alloy powder morphology (a) and morphology of the same powder plus 5% Al_2O_3 (b).

3.2 Microstructural and phase analysis of pure CoCr alloy powder for forming sample parts

The sample surface and grain structures after molding were observed by SEM. The crystal structure appeared relatively uniform and compact after molding (Fig. 3a). However, there were also visible flaws under 1000X magnification, like the local area uplift phenomenon seen in Fig. 3b. The reason for this was that, during the forming process, impurities were present in the powder, which rendered the powder uneven or led to the formation of tiny masses, resulting in local volumes that lack sufficient density. The microstructural orientation of the CoCr alloy showed no obvious macro-defects, such as pores and cracks on the surface of the sample (Fig. 3c). This showed that densification of the formed part or piece under this method was high.

At temperatures above 417°C, the matrix of the Co-based alloy formed the γ-phase (also called austenite) of the fcc structure, and the γ-phase of the fcc structure was converted to the γ-phase with its allotrope ε-phase. As the γ-phase was thermodynamically unstable, $\gamma \rightarrow \varepsilon$ phase transformation occurred during laser melting of the selected area. In this study, selective laser melting, such as single-pass

scanning of CoCr alloy powder, resulted in a rapid-melting and rapid-solidification process.

The Co-base alloy, rapidly melted by laser heating, did not undergo phase transformation and remained in γ-Co phase. This was because the rapid cooling of the substrate to room temperature caused γ-Co phase to be retained due to the phase change. This observation, combined with XRD analysis, indicates that the final phase of the CoCr alloy produced γ-Co and carbide phases. The main phase transformation involved the formation of carbide resulting from the formation of fine columnar γ-Co grains composed of cellular dendrites from Cr, and also the formation of Mo dendrite during rapid solidification (Formula 1). Therefore, carbon also moved into the inter-dendritic regions and grain boundaries[24].

$$\gamma - \mathrm{Co} \rightarrow \gamma' + + M_{23}\mathrm{C}_6 + M_6\mathrm{C} \qquad (1)$$

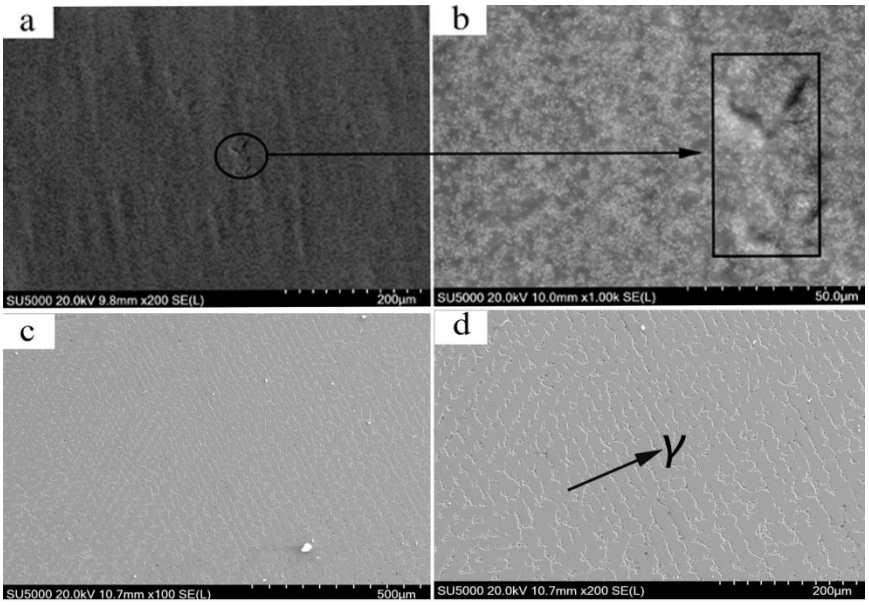

Fig. 3. SEM micrograph of pure CoCr alloy powder molding.

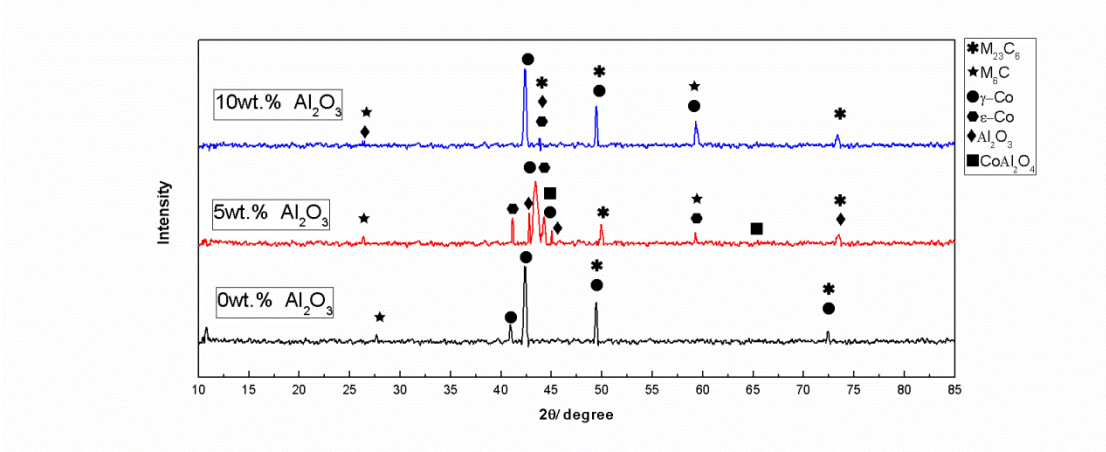

Fig. 4. XRD patterns of the CoCr alloy sample with 0, 5, and 10% Al_2O_3.

Further analysis of the microstructure of the alloys, revealed that the metallographic structure of a single-channel scanned CoCr alloy specimen was composed of austenite and a carbide-like structure (Fig. 5a). Its crystal structure was columnar crystalline, with carbide distributed in the grain boundaries, and some agglomeration occurring in the material's internal structure (Fig.5b). The microstructures consisted of a Co-based solid solution and an agglomerated second phase, which was shown by XRD analysis to be a carbide phase. There were generally two types of carbonized structures in CoCr alloys, $M_{23}C_6$ and M_6C, in which M_6C carbide was rich in Mo, while $M_{23}C_6$ was rich in Cr[25]. From energy-dispersive X-ray spectroscopic (EDS) results, it was speculated that one area was a Mo-rich M_6C carbide and reticular while another was a Cr-rich $M_{23}C_6$-type carbide (mainly $Cr_{23}C_6$; Fig. 5b, points 1 and 2, respectively).

The correct amount of carbon can form carbides with the corresponding elements in Co-based alloys. Those carbides have long been considered as major strengthening phases in Co-based alloys[26-28]. The existence of these carbides affects the materials' mechanical properties, wear resistance, corrosion resistance, and biocompatibility, in

addition to the improvement in the CoCr alloy mechanical properties.[25,29] Thus, the next step was to analyze how to improve the mechanical and biological properties of CoCr alloys by controlling the amount of carbide in the alloy.

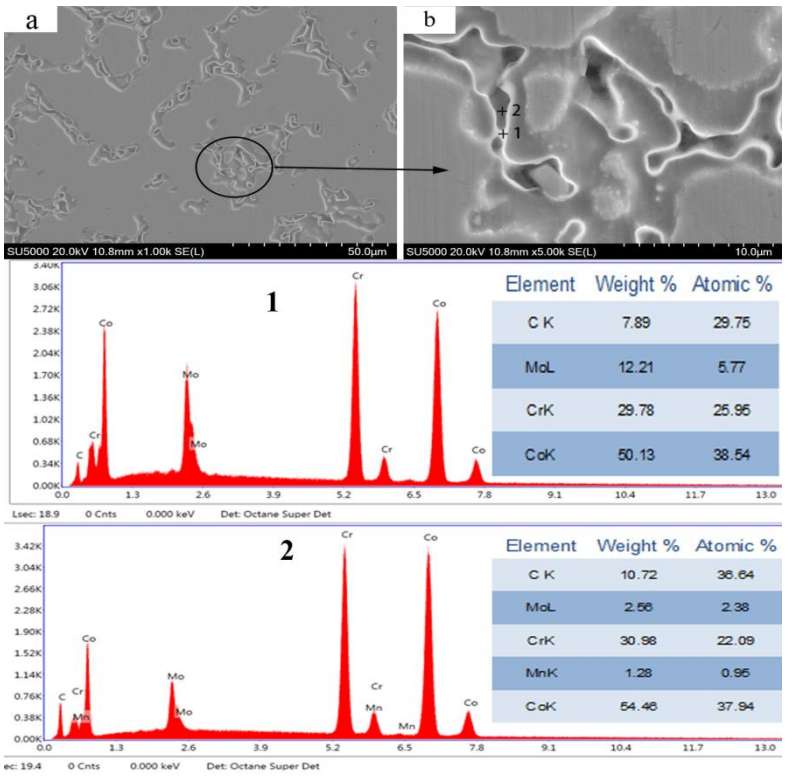

Fig. 5. Microstructure of 0% added Al_2O_3 samples, and EDS analysis.

3.3 Microstructural and phase analysis of alloy powder molded parts after Al_2O_3 addition

XRD analysis revealed that the alloy phases after the addition of Al_2O_3 were γ-C_O, ε-Co, $M_{23}C_6$, M_6C, Al_2O_3, and $CoAl_2O_4$ (Fig. 4). Compared to pure CoCr alloy, the XRD diffraction pattern of the alloy with Al_2O_3 content of 5% showed that the main phase peak weakened, the angle shifted to the right, the carbide result changed, and the M_6C phase increased. At this time, ε-Co appeared, compared relative to the γ phase without Al_2O_3 because of the lower thermal conductivity of Al_2O_3 (10.022 $W \cdot m^{-1} \cdot K^{-1}$, 1200°C). During the melting-cooling process, the large amounts of fine

Peer-reviewed version available at Metals 2019, 9, 1074; doi:10.3390/met9101074

Al_2O_3 particles contained in the crystals and crystal fronts (Fig. 7), hindered heat transfer not only from the liquid, but also from the solid part of the solidification, eventually causing a portion of the γ-Co to convert to ε-Co particles at a slower cooling rate. The main phase of the reaction is shown in Formula 2.

$$\gamma - \mathrm{Co} \rightarrow \gamma' + \varepsilon' + M_{23}C_6 + M_6C + \mathrm{Al_2O_3} + \mathrm{CoAl_2O_4} \qquad (2)$$

Comparing Figures 6 and 3d, it can clearly be seen that the alloy structure was still columnar crystalline after Al_2O_3 addition, but the columnar grains were visibly smaller, and even smaller than those without Al_2O_3 addition. Also, a large amount of carbide disappeared and Al_2O_3 agglomeration areas appeared.

When the Al_2O_3 content was 5%, the grain boundaries were the most visible in the microstructure, with the columnar grains small in size, and the structures similar to equiaxed grains (Fig. 6a–6d). Carbide accumulation areas were almost undetectable, and the microstructure and properties of the characterized parts are therefore judged to be the best when Al_2O_3 content was 5%. Further analysis was carried out on characterized parts, and grain boundaries observed under magnification, which revealed that in local areas are similar to the cellular structure, and that the columnar grain structure disappeared, (Fig 8a, point 1). In the deep regions of the material with Al_2O_3 particles (Fig. 8a, point 3), it was seen, from the backscatter plot of Figure 8b, that the black areas were precipitated Al_2O_3 particles, whereas the bright white areas were composed of carbide. According to EDS results, in Figure 8a, point one was Mo-rich M_6C and point two Cr-rich $M_{23}C_6$. When compared with a non-Al_2O_3 alloy, the carbon content in these two points was significantly reduced, the carbide grain

size was small, and the position where it occurred changed, and did not take the form of a mesh or sheet, but became granular. The conclusion here was that the addition of Al_2O_3 to the alloy reduced the final carbide content of the molded part. This is due to In CoCr alloys, γ-Co grains themselves have heavy faulting, which creates the nucleation centers for carbides in CoCr alloys[30]. In this study, adding Al_2O_3 caused the final morphology of γ-Co grains to change during the nucleation process. Due to the fine structure, it is inferred that the stacking faults of γ-Co grains were reduced along with carbide nucleation, which changed the time and amount of carbides produced.

In Figure 8a, point 3 and area A were examined using EDS, and Al and O were detected there. Considering these results in combination with XRD analysis (Fig. 4), we conclud that the amount of carbides was further reduced. Al was a solid solution in the Co-based solid solution, the main phase of the peak slowly weakened, the angle shifted to the right, the carbide results changed, and the M_6C phase increased. M_6C carbides have been reported to have good thermal stability, and $M_{23}C_6$ carbides were shown to convert to M_6C at a solution temperature of 1165°C[31]. During the laser cladding process, there was a heat-effected zone that led to the conversion of $M_{23}C_6$ carbide to M_6C type. Furthermore, the addition of Al_2O_3 reduced the nucleation sites of $M_{23}C_6$ carbides, created the proper conditions for the conversion of $M_{23}C_6$ to M_6C.

When the Al_2O_3 content was 7.5%, columnar crystals increased (Fig. 6c), but the arrangement was chaotic and the overall structural properties not as good as those with 5% Al_2O_3. When the Al_2O_3 content was further increased to 10%, the

microstructure remained columnar (Fig. 9a). By comparison with XRD analysis (Fig. 4), we see that the main peak becomes taller and narrower with more carbide. There were still deep areas similar to those found in the previous alloy (Fig. 9b), where carbides were present in a manner similar to those without Al_2O_3 (Fig. 9, 1 points). The elemental distributions at points 1 and 2 were detected by EDS scanning, showed that in deep regions (points 1 and 2) the elements were different from the previous alloy (Fig. 8), the Al disappeared, and C content increased. The C content also significantly increased at other points. The analysis of the elemental distributions at points 1 and 2 in Fig. 9 revealed that the elements at these points were essentially the same as those in the pure CoCr alloy.

The existence of Al_2O_3 particles clearly changed the CoCr alloy's microstructure. The reason for these results was that Al_2O_3 has a small particle size, large surface energy, and high melting point. When Al_2O_3 particles were added in small amounts, they were uniformly distributed in the liquid metal (Fig. 7), which not only increased the degree of super-cooling but also promoted spontaneous nucleation at the front of columnar solidification and hindered dendrite growth. During rapid solidification and crystallization, a portion of Al_2O_3 particles was in the solid solution, and some nucleation occurred spontaneously at the solid-liquid interface (Fig. 10). Because of the large surface effects by Al_2O_3 particles, they accessed atoms from the surrounding metal liquid and grew after nucleation. As was observed in Figure 8b, part of the Al_2O_3 particle agglomeration resided in the columnar stem, and part of the columnar front obstructed the crystal growth. The reason for the observed agglomeration was

that Al_2O_3 was larger in area than the surface area, and was absorbed very easily onto material surfaces.

When the Al_2O_3 content was increased to 10% and Al_2O_3 particles increased, the solid solution was rapidly contacted with more Al_2O_3 particles, which grew as nuclei. The contacting particles were not in the form of solid nuclei but as solid solution particles. These large and elongated particles had different orientations in the columnar crystal structure, and interlocked with each other. Since it is very easy to induce cracks in these interlocking regions during processing, the mechanical properties were significantly reduced. In several samples with 10% Al_2O_3 content, the comprehensive analysis of the microstructural properties was the worst. In summary, the microstructure and properties of the alloy were the best when 5% Al_2O_3 was added.

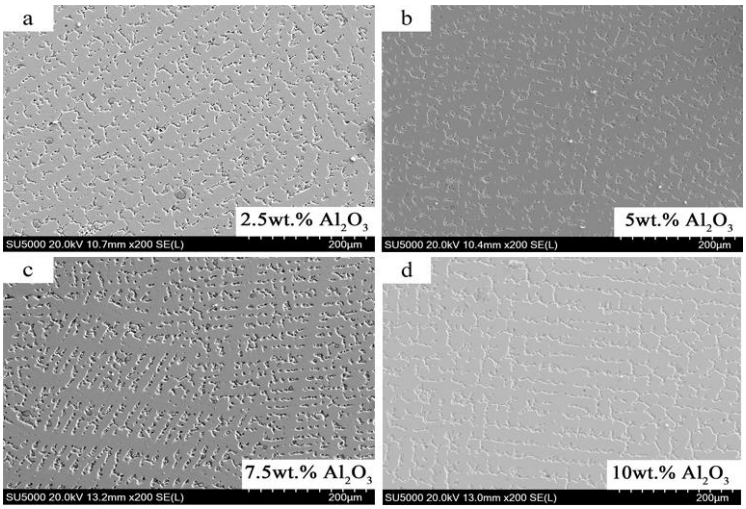

Fig. 6. SEM micrograph of Al_2O_3 molded parts.

Preprints (www.preprints.org) | NOT PEER-REVIEWED | Posted: 2 September 2019 doi:10.20944/preprints201909.0025.v1

Peer-reviewed version available at Metals 2019, 9, 1074; doi:10.3390/met9101074

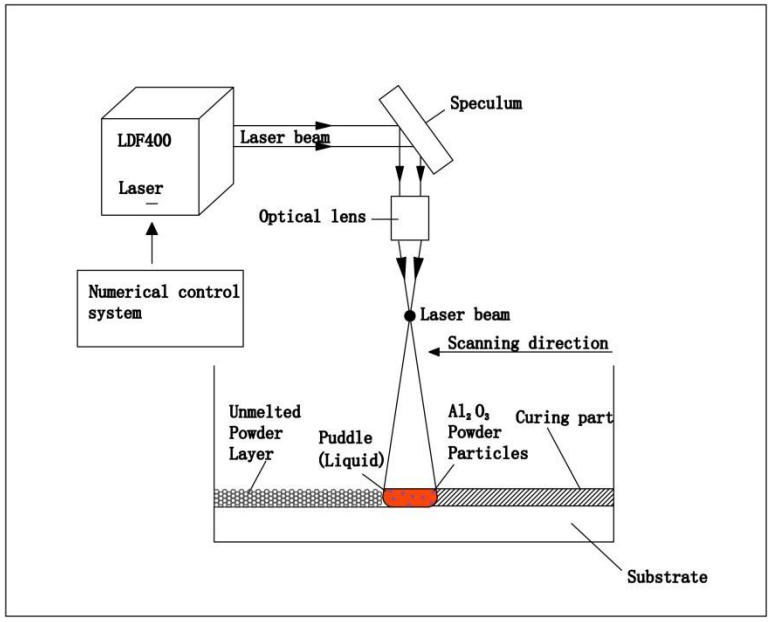

Fig. 7. Constituency laser melting process diagram.

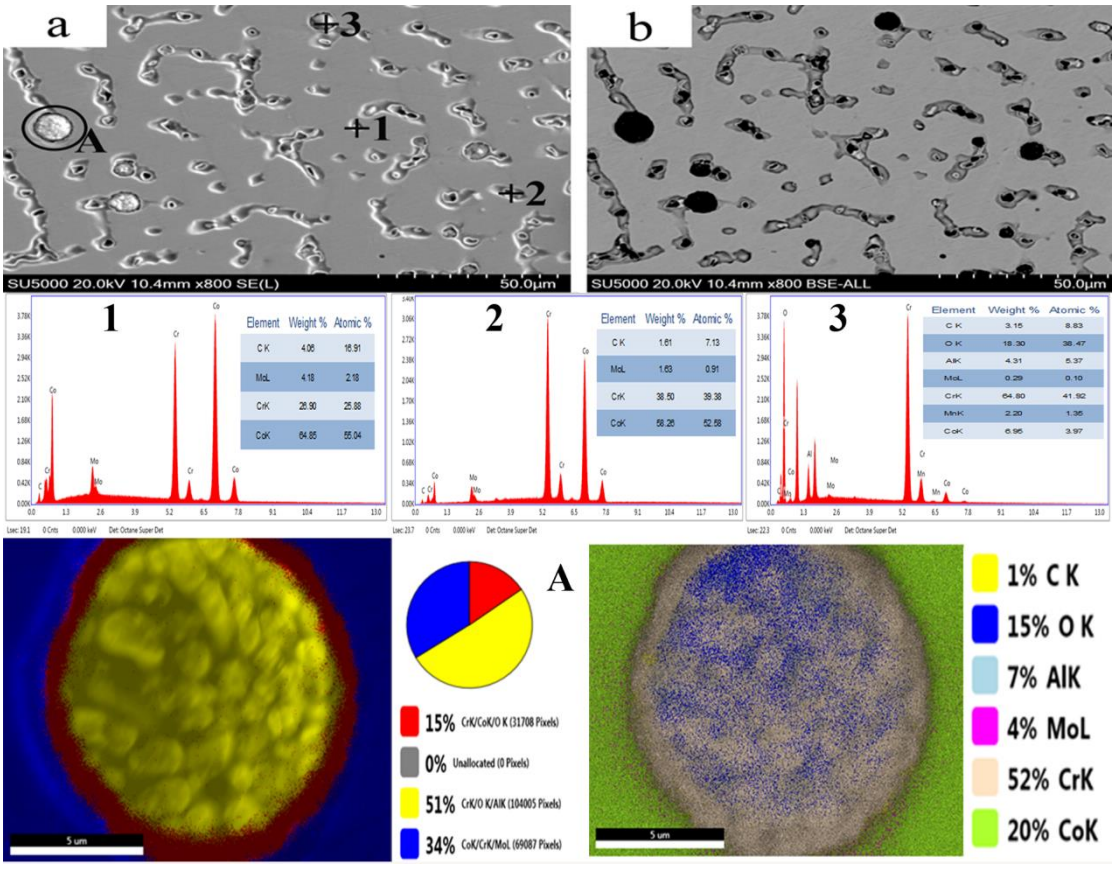

Fig. 8. Microstructural analysis of 5% Al_2O_3.

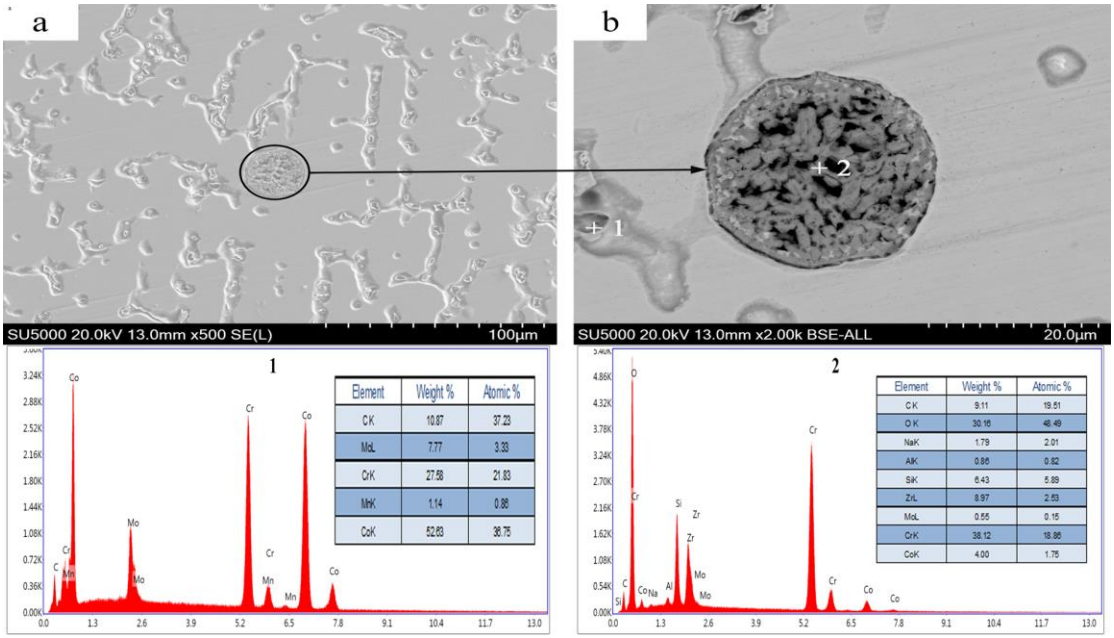

Fig. 9. Microstructural analysis of 10% Al_2O_3.

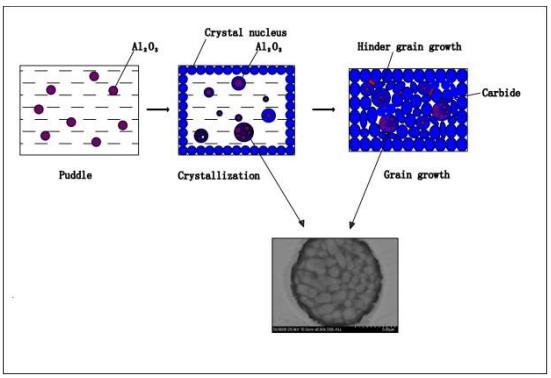

Fig. 10. Modified sample crystallization process diagram (5% wt. Al_2O_3).

3.4 Mechanical properties

The hardness of 5% CoCr alloy from the boundary to the center was the best of the several alloys, with an average Vickers hardness of 338.775HV, which corresponded to 335 HV of the CoCr alloy tooth standard, slightly above the standard specification (Fig. 11).

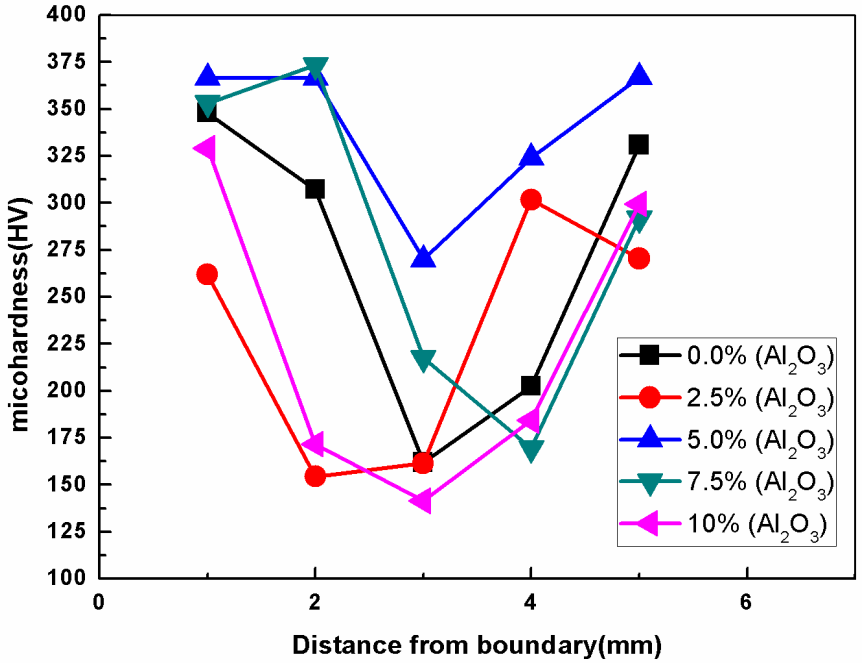

Fig. 11. Microhardness distribution of CoCr alloy doped with different Al_2O_3 percentages.

The representative stress-strain curves of CoCr alloy doped with different Al_2O_3 percentages shows that the tensile properties of CoCr alloy were the best when the content of Al_2O_3 was 5%, reaching a value of 856 MPa, which was markedly higher than the minimum value (665 MPa) recommended in ISO5832-4 and GB17100 (Fig. 12). Furthermore, the specimen also exhibited a high elongation-to-failure percentage of 12.79%, while ISO5832-4 specifies that the minimum requirement for elongation is 8%.

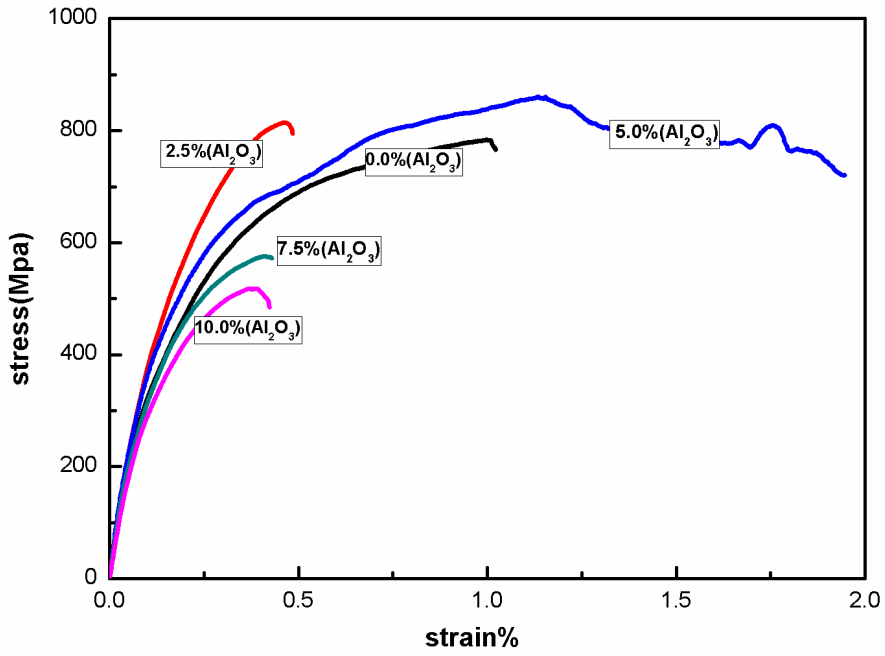

Fig. 12. Stress-strain curves of CoCr alloy doped with different Al_2O_3 percentages.

The tensile strength of alloy specimens with 5% Al_2O_3 was tested, and the fracture surfaces examined at different magnifications, showed that the former interface between powder particles could not be distinguished, indicating that the alloy achieved full metallurgical bonding (Fig. 13a). In addition, a mixture of smooth and rough zones was observable, with the presence of a high portion of rough regions indicative of predominantly ductile fracture [32]. The fracture surfaces of the alloy had parabolic tearing edges and dimple-like structures (Fig. 13a and 13b, respectively), suggesting ductile tendency quasi-cleavage fracture[22]. It appeared that the alloy ductility was improved when local plastic zone appeared during fracture.

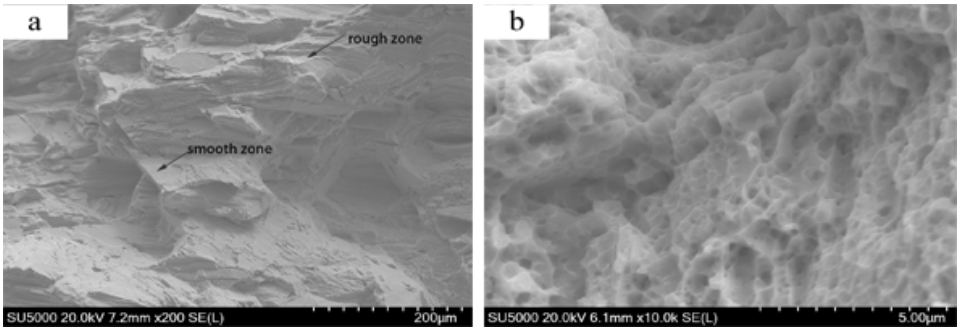

Fig. 13. Micrographs of fracture surfaces of tensile specimens containing 5%Al_2O_3.
(a) Fracture surface of tensile specimens
(b) The magnified fracture surface of Fig.13(a)

K. Yamanaka has studied high entropy alloys [24], and found that carbides ($M_{23}C_6$ and M_6C) are much harder than the surrounding γ-substrates, and tend to strengthen the alloy. In this study, when the Al_2O_3 content was 5%, the alloy microstructure and carbide morphology were changed on one hand, and the carbide morphology changed on the other, which enhanced the alloy's microhardness and elongation. In addition, the microstructures were mainly fine columnar crystals, thus producing higher ultimate tensile strength. The carbide content increased with the increase of content, but the grain size was coarse, which resulted in the deterioration in the mechanical properties of the CoCr alloy.

We found that after adding 5% Al_2O_3, the microstructure of the alloy became finer, and played the role of fine grain strengthening. It is precisely under this effect that the mechanical properties of the alloy were improved remarkably. Also, the γ-Co grain boundary might have provided a rapid diffusion path for Cr and Mo. and due to enhanced diffusion, the carbide eutectic structure was very hard, and the carbides dispersed in the eutectic phase existed at the interface, which improved the alloy's strength and hardness. Therefore, the introduction of 5% Al_2O_3 was an effective way

Peer-reviewed version available at Metals 2019, 9, 1074; doi:10.3390/met9101074

of improving the mechanical properties of the CoCr alloy. Therefore, this study provided insight for improving the wear properties and biocompatibility of CoCr alloys.

3.5 Formation Mechanism of the $CoAl_2O_4$ Phase

The formation of an alloy from mixed powders after the addition of Al_2O_3, showed that the mixture was melted (Fig. 14a). As the temperature increased, Co and O reacted to form CoO, while the diffusion of Cr and Mo began to occur (Fig. 14b), then the previously formed CoO and Al_2O_3 reacted to form $CoAl_2O_4$ (Figs. 14c and 14d).

The appearance of the $CoAl_2O_4$ phase might also have been due to the fact that Al_2O_3 particle bonds were not saturated, and that new nucleation centers in the molten pool were growing. As the nucleation centers grew, the O and Co in the alloying material were adsorbed and combined during the growth process.

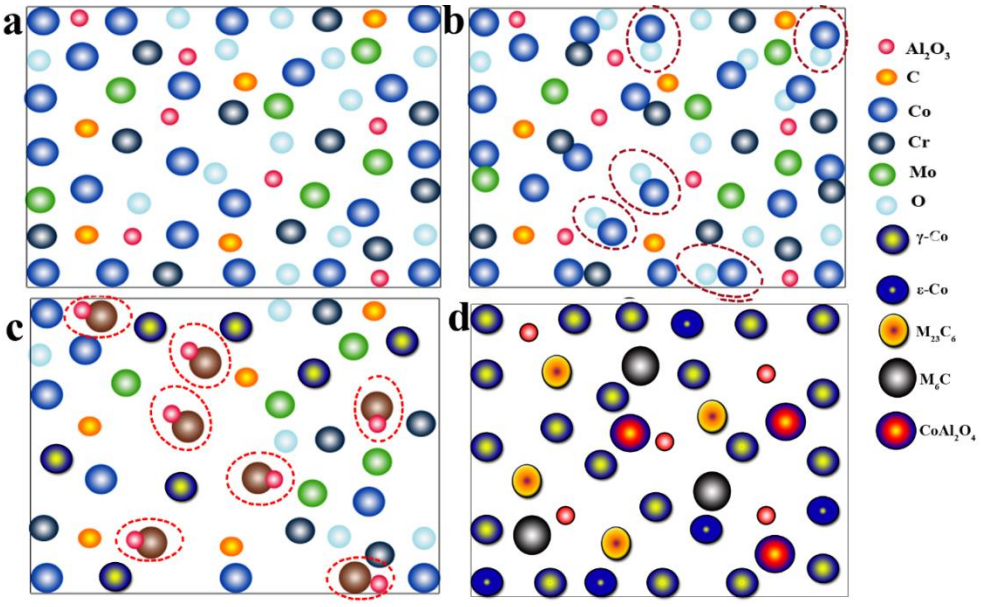

Fig. 14. Compound formation process.

The following reactions were inferred to occur during laser cladding:

$$Co + O \rightarrow CoO \quad (3)$$

$$CoO + Al_2O_3 \rightarrow CoAl_2O_4 \quad (4)$$

We calculated Gibbs free energy of reaction (3) at 298~2000K by referring to Thermochemical Data of Pure Substances[33]. The results show that reaction (3) can be carried out spontaneously, which indicates that the reaction is easy to proceed (In Fig. 15). Due to the strong interactions between Co and Al_2O_3, a cobalt acicular spinel compound was easily produced, and was difficult to reduce[34], meaning that reaction (4) occurred easily as well, and that the resulting $CoAl_2O_4$ allowed the final morphology to assume the fine microstructure observed in the present study.

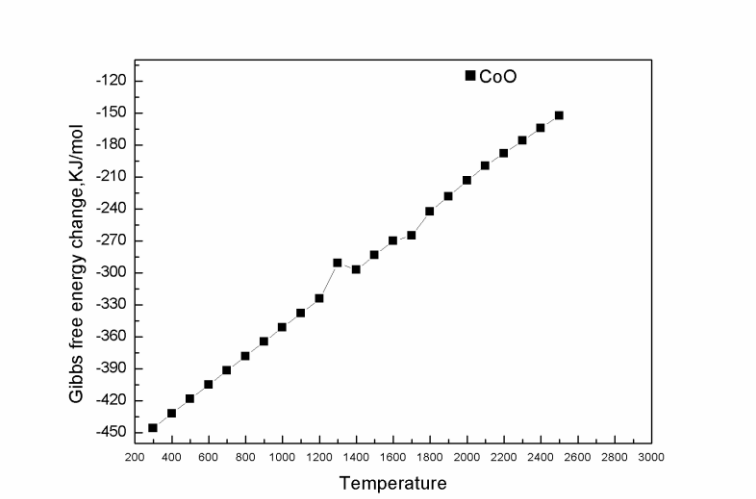

Fig. 15. Gibbs Free Energy of reaction at different temperatures.

4. Conclusion

This work mainly studies on the powder properties and molding properties of CoCr alloy with adding different proportion of Al_2O_3 were studied, and compared with pure CoCr alloy, the following conclusions were drawn.

（1）Among all the ratios, the microstructure and mechanical properties of the alloy are the best when the content of Al_2O_3 is 5%. At this time, the deep region of Al_2O_3 particles Al_2O_3 particles appears in the microstructure of the alloy, which

hinders the growth of dendrite. These results showed the columnar grain size of the alloy obviously smaller than that of the alloy of without adding Al_2O_3.

（2）With the addition of Al_2O_3, the accumulation area of carbides in the microstructure of the alloy almost disappeared and the M_6C phase increased, which indicates the change of microstructure and morphology of CoCr alloy.

（3）The average Vickers hardness of the alloy mixed with 5% Al_2O_3 is 338.775 HV, and the tensile strength is 856 MPa. From the fracture morphology analysis of the alloy, it is concluded that the local plastic zone appears during the fracture of the alloy. It suggests that the mechanical properties of the alloy are improved.

5. Acknowledgments

This research work was supported by Primary Research and Development Plan of Shanxi Province (Grant No. 201603D121020-1). The authors are grateful for these grants.

References

1. Handbook of Materials for Medical Devices, https://www.researchgate.net/publication/313151336_Handbook_of_Materials_for_Medical_Devices
2. J. Li, C. Chen, J. Liao, L. Liu, X. Ye, S. Lin, J. Ye, Bond strengths of porcelain to cobalt-chromium alloys made by casting, milling, and selective laser melting, *J Prosthet Dent*, **118**(1), 69-75 (2017)
3. A 5-Year Retrospective Study of Cobalt-Chromium–Based Fixed Dental Prostheses, http://www.quintpub.com/journals/ijp/abstract.php?iss2_id=1129&article_id=13320&article=8&title=A%205-Year%20Retrospective%20Study%20of%20Cobalt-Chromium%96Based%20Fixed%20Dental%20Prosthesesxx
4. Y.S. Al Jabbari, T. Koutsoukis, X. Barmpagadaki, S. Zinelis, Metallurgical and interfacial characterization of PFM Co-Cr dental alloys fabricated via casting, milling or selective laser melting, *Dent Mater*, **30**(4), e79-88 (2014)
5. U. Malayoglu, A. Neville, Mo and W as alloying elements in Co-based alloys—their effects

on erosion–corrosion resistance, *Wear*, **259**(1-6), 219-229 (2005)

6. K. Quante, K. Ludwig, M. Kern, Marginal and internal fit of metal-ceramic crowns fabricated with a new laser melting technology, *Dent Mater*, **24**(10), 1311-1315 (2008)
7. T. Traini, C. Mangano, R.L. Sammons, F. Mangano, A. Macchi, A. Piattelli, Direct laser metal sintering as a new approach to fabrication of an isoelastic functionally graded material for manufacture of porous titanium dental implants, *Dent Mater*, **24**(11), 1525-1533 (2008)
8. V. Alt, M. Hannig, B. Wostmann, M. Balkenhol, Fracture strength of temporary fixed partial dentures: CAD/CAM versus directly fabricated restorations, *Dent Mater*, **27**(4), 339-347 (2011)
9. Y.S. Hedberg, B. Qian, Z. Shen, S. Virtanen, I.O. Wallinder, In vitro biocompatibility of CoCrMo dental alloys fabricated by selective laser melting, *Dent Mater*, **30**(5), 525-534 (2014)
10. B. Qian, K. Saeidi, L. Kvetkova, F. Lofaj, C. Xiao, Z. Shen, Defects-tolerant Co-Cr-Mo dental alloys prepared by selective laser melting, *Dent Mater*, **31**(12), 1435-1444 (2015)
11. N. Poolphol, T. Sakkaew, K. Kachin, P. Jantaratana, W. Vittayakorn, Physical, mechanical and magnetic properties of cobalt-chromium alloys prepared by conventional processing, *Materials Today: Proceedings*, **4**(5), 6358-6364 (2017)
12. K.C. Li, D.J. Prior, J.N. Waddell, M.V. Swain, Comparison of the microstructure and phase stability of as-cast, CAD/CAM and powder metallurgy manufactured Co-Cr dental alloys, *Dent Mater*, **31**(12), e306-315 (2015)
13. S. Yager, J. Ma, H. Ozcan, H.I. Kilinc, A.H. Elwany, I. Karaman, Mechanical properties and microstructure of removable partial denture clasps manufactured using selective laser melting, *Additive Manufacturing*, **8**, 117-123 (2015)
14. O.B.M.d.G.C.d.M.R.R.J.M.D.d.A. Rollo, Effect of beryllium on the castability and resistance of ceramometal bonds in nickel-chromium alloys 《*Journal of Prosthetic Dentistry*》, **80**(5), 570-574

(1998)

15. H.M. Ayu, S. Izman, R. Daud, G. Krishnamurithy, A. Shah, S.H. Tomadi, M.S. Salwani, Surface Modification on CoCrMo Alloy to Improve the Adhesion Strength of Hydroxyapatite Coating, *Procedia Engineering*, **184**, 399-408 (2017)
16. R.I.M. Asri, W.S.W. Harun, M. Samykano, N.A.C. Lah, S.A.C. Ghani, F. Tarlochan, M.R. Raza, Corrosion and surface modification on biocompatible metals: A review, *Mater Sci Eng C Mater Biol Appl*, **77**, 1261-1274 (2017)
17. M. Mori, N. Sato, K. Yamanaka, K. Yoshida, K. Kuramoto, A. Chiba, Development of microstructure and mechanical properties during annealing of a cold-swaged Co-Cr-Mo alloy rod, *J Mech Behav Biomed Mater*, **64**, 187-198 (2016)
18. P. Mengucci, G. Barucca, A. Gatto, E. Bassoli, L. Denti, F. Fiori, E. Girardin, P. Bastianoni, B. Rutkowski, A. Czyrska-Filemonowicz, Effects of thermal treatments on microstructure and mechanical properties of a Co-Cr-Mo-W biomedical alloy produced by laser sintering, *J Mech Behav Biomed Mater*, **60**, 106-117 (2016)
19. K. Yamanaka, M. Mori, A. Chiba, Nanoarchitectured Co-Cr-Mo orthopedic implant alloys: nitrogen-enhanced nanostructural evolution and its effect on phase stability, *Acta Biomater*, **9**(4), 6259-6267 (2013)
20. D. Kotoban, A. Nazarov, I. Shishkovsky, Comparative Study of Selective Laser Melting and

Direct Laser Metal Deposition of Ni 3 Al Intermetallic Alloy, *Procedia IUTAM*, **23**, 138-146 (2017)

21. J. Cai, G.P. Nordin, S. Kim, J. Jiang, Surface properties and corrosion behavior of Co-Cr alloy fabricated with selective laser melting technique, *Cell Biochemistry & Biophysics*, **67**(3), 983-990 (2013)
22. A. Takaichi, Suyalatu, T. Nakamoto, N. Joko, N. Nomura, Y. Tsutsumi, S. Migita, H. Doi, S. Kurosu, A. Chiba, N. Wakabayashi, Y. Igarashi, T. Hanawa, Microstructures and mechanical properties of Co-29Cr-6Mo alloy fabricated by selective laser melting process for dental applications, *J Mech Behav Biomed Mater*, **21**, 67-76 (2013)
23. K. Hagihara, T. Nakano, K. Sasaki, Anomalous strengthening behavior of Co–Cr–Mo alloy single crystals for biomedical applications, *Scripta Materialia*, **123**, 149-153 (2016)
24. <钴铬铝合金 1-s2.0-0025541687903958-main.pdf>,
25. E. Bettini, T. Eriksson, M. Boström, C. Leygraf, J. Pan, Influence of metal carbides on dissolution behavior of biomedical CoCrMo alloy: SEM, TEM and AFM studies, *Electrochimica Acta*, **56**(25), 9413-9419 (2011)
26. K. Huang, K. Marthinsen, Q. Zhao, R.E. Logé, The double-edge effect of second-phase particles on the recrystallization behaviour and associated mechanical properties of metallic materials, *Progress in Materials Science*, **92**, 284-359 (2018)
27. Y. Liao, R. Pourzal, P. Stemmer, M.A. Wimmer, J.J. Jacobs, A. Fischer, L.D. Marks, New insights into hard phases of CoCrMo metal-on-metal hip replacements, *J Mech Behav Biomed Mater*, **12**, 39-49 (2012)
28. A. Chiba, K. Kumagai, N. Nomura, S. Miyakawa, Pin-on-disk wear behavior in a like-on-like configuration in a biological environment of high carbon cast and low carbon forged Co–29Cr–6Mo alloys, *Acta Materialia*, **55**(4), 1309-1318 (2007)
29. C. Song, M. Zhang, Y. Yang, D. Wang, Y. Jia-kuo, Morphology and properties of CoCrMo parts fabricated by selective laser melting, *Materials Science and Engineering: A*, **713**, 206-213 (2018)
30. <真五 Review of ceramics.pdf>,
31. C. Rao, EFFECT OF HEAT TREATMENT ON CORROSION BEHAVIOR OF WELD DEPOSITED Co-Cr-Mo ALLOY, *ARPN Journal of Engineering and Applied Sciences*, (2016 , 11 (20) :), 12188-12191
32. X. Xian, Z. Zhong, B. Zhang, K. Song, C. Chen, S. Wang, J. Cheng, Y. Wu, A high-entropy V 35 Ti 35 Fe 15 Cr 10 Zr 5 alloy with excellent high-temperature strength, *Materials & Design*, **121**, 229-236 (2017)
33. I.B.G. Platzki, <纯物质热化学数据手册　上卷.pdf>,
34. A. Tavasoli, S. Karimi, S. Taghavi, Z. Zolfaghari, H. Amirfirouzkouhi, Comparing the deactivation behaviour of Co/CNT and Co/γ-Al2O3 nano catalysts in Fischer-Tropsch synthesis, *Journal of Natural Gas Chemistry*, **21**(5), 605-613 (2012)